Japanese Journal of Applied Physics

The Japan Society of Applied Physics

ACCEPTED MANUSCRIPT

Controllability of luminescence wavelength from GeSn wires fabricated by laser-induced local liquid phase crystallization on quartz substrates

To cite this article before publication: Takayoshi Shimura *et al* 2023 *Jpn. J. Appl. Phys.* in press https://doi.org/10.35848/1347-4065/acb9a2

Controllability of luminescence wavelength from GeSn wires fabricated by laser-induced local liquid phase crystallization on quartz substrates

Takayoshi Shimura[1]*, Ryoga Yamaguchi[1], Naoto Tabuchi[1], Masato Kondoh[1], Mizuki Kuniyoshi[2], Takuji Hosoi[3], Takuma Kobayashi[1], and Heiji Watanabe[1]

[1]*Graduate School of Engineering, Osaka University, 2-1 Yamadaoka, Suita, Osaka 565-0871, Japan*

[2]*ULVAC-Osaka University Joint Research Laboratory for Future Technology, 2-1 Yamadaoka, Suita, Osaka 565-0871, Japan*

[3]*School of Engineering, Kwansei Gakuin University, Sanda, Hyogo, Japan*

E-mail: shimura@prec.eng.osaka-u.ac.jp

We examined the effects of the laser scan speed and power on the Sn fraction and crystallinity of GeSn wires of 1 μm width and 1 mm length fabricated by laser-induced local liquid phase crystallization on quartz substrates. The Sn fraction increased from 1 to 3.5% with an increasing scan speed from 5 to 100 μm/s, corresponding to a luminescence wavelength of 1770–2070 nm. This result can be interpreted as the scan speed dependence of the non-equilibrium degree during crystal growth. The increase in the laser power reduced the Sn fraction and caused a blue shift in the luminescence wavelength. We discuss these phenomena based on the growth kinetics of zone melting.

1. Introduction

Silicon photonics is a technology that integrates optical devices using microfabrication technology, which has been developed as silicon technology[1)–4)]. Optical and electronic circuits can be integrated, and various applications for optical communication, quantum computing[5)], quantum cryptography[6)], artificial intelligence[7)], and environmental/biological sensing[8),9)] are being investigated. Commercially available optical transceivers supporting a 400 Gbps optical link in the data center already exist[10)]. However, light sources are made of group III–V materials of InP, and they are stacked by a bonding process[11)]. If the light source can be formed from group IV elements, such as Ge, then a broader range of applications is expected because of the significant cost reduction.

Ge is an indirect-bandgap semiconductor, similar to Si; however, the energy difference at the bottom of the conduction band between the Γ and L points is only 136 meV[12)]. Therefore, various studies to improve the optical properties of Ge are underway[13),14)]. When tensile strain is applied in the in-plane direction of the Ge layers, the bottom of the conduction band decreases; however, the Γ point decreases more rapidly than the L point, resulting in a direct-bandgap semiconductor. The same effect can be obtained by adding Sn atoms, which are also Group IV elements[15)–17)]. In addition, the light emission efficiency is improved by high n-type doping[18)].

However, many problems are to be resolved when growing single-crystal GeSn layers. The lattice mismatch between Ge and Si crystals is 4%, and a two-step growth process is generally used with low-temperature growth in the initial stage to suppress crystal defects[19),20)]. Although threading dislocations significantly decrease, the density is still maintained at approximately $10^6/cm^2$, and crosshatch patterns are observed on the growth surface, even after forming the 2.5-μm thick Ge layer[21)]. The addition of Sn atoms to the Ge layer made this even more complex. Moreover, lattice mismatch occurs on relaxed Ge substrates, and compressive strain is applied, mitigating the effect of Sn addition. Furthermore, the solid solubility of Sn atoms in Ge is considerably low (approximately 1%), and low-temperature non-equilibrium growth at several hundred °C is inevitable for the growth of GeSn films with Sn fractions exceeding the solid solubility[22)]. This results in significantly poor optical properties owing to non-radiative recombination through point defects[23)].

To overcome these issues, local liquid-phase crystallization (LLPC) to fabricate high-quality single-crystal GeSn wires with high tensile strain is being developed[24)–29)]. In this method, an amorphous GeSn wire, typically 2 μm wide, on an amorphous SiO_2 substrate is melted at a temperature above the melting point of the GeSn wire but remains unmelted at one end of the wire. LLPC starts from the interface with the unmelted GeSn wire during cooling. This method has the benefit of partial melting comparing to the similar methods.[30),31)]

This method has three main advantages. First, defects and compressive strain originating from lattice mismatch with the substrates are eliminated. Second, tensile strain is induced in the GeSn wires owing to the difference in the thermal expansion coefficients of the GeSn wires and substrate. Third, the Sn fraction over the solubility owing to the non-equilibrium growth caused by the high growth speed is high. GeSn wires with tensile stress of approximately 0.5% and Sn fraction of 2.6–5.4% have been validated[24),25)]. Notably, the tensile strain induced by this method is independent of the Sn fraction in GeSn wires, enabling GeSn wires to have a high Sn fraction and tensile strain.

Currently, a laser-induced LLPC to enhance the controllability of GeSn growth (Fig. 1) is being developed[32)]. The laser-induced LLPC offers the advantage of GeSn wires exhibiting single crystal structure over the entire substrate via repeated laser scan compared with the LLPC via rapid thermal annealing (RTA) using partial carbon susceptors. In addition, the crystal growth speed can be controlled by changing the laser scan speed. Whereas, in the RTA method, although the temperature of the carbon susceptor can be controlled, the growth speed cannot be controlled precisely.

The laser-induced LLPC corresponds to zone melting[33)], which is commonly used to grow bulk crystals and control impurities in materials; however, our method is on the micrometer scale, making it unique. In this method, the region illuminated by the laser light is melted and moves with the laser scan. The Sn fraction in the liquid region is determined by the balance between the incoming and outgoing Sn atoms. The incoming Sn atoms are determined based on the initial Sn concentration in the amorphous region. The outgoing Sn atoms depend on the segregation coefficient (the ratio of the Sn fraction in the crystal to that in the liquid region) and the Sn fraction in the liquid region. Hence, we obtain the following differential equation:

$$wdC_L = -kC_L dx + C_0 dx,$$

where w is the zone width, C_L is the Sn concentration in the liquid region, k is the segregation coefficient, and C_0 is the initial Sn concentration of the amorphous GeSn wire. Ideally, the solution of this differential equation is expressed as:

$$C_s(x) = C_0\left\{1 - (1-k)e^{-\frac{kx}{w}}\right\},$$

where C_s is the Sn concentration in the crystal GeSn wires. However, the equation is more complex in reality. Therefore, this study investigates the effects of the scan speed and laser power on the Sn fraction and crystallinity of GeSn wires to validate the fundamental phenomenon during laser-induced LLPC. We demonstrate the effects of laser-induced LLPC along with previously reported results[34] and discuss them based on the growth kinetics of zone melting.

2. Experimental methods

Commercially available 20×20 mm^2 quartz substrates were cleaned by Piranha solution. Amorphous GeSn layers with a thickness of 200 nm were formed at 300°C on quartz substrates by molecular beam deposition. The base pressure of the deposition chamber was less than 5×10^{-10} torr. The Sn fraction is approximately 2% inside the film. However, many Sn atoms segregate on the surface; thus, the total Sn fraction is much larger than 2%[24),27)]. Wire patterns of 1 μm width, 1 μm space, and 1 mm length were fabricated using photolithography and reactive ion etching. The area of each pattern is 0.5 × 1 mm. Laser-induced LLPC was performed after capping with SiO_2 of 1 μm thick via sputter deposition. The wavelength of the CW laser light was 808 nm, and the illumination area was approximately 0.16 × 3 mm; hence, the zone width was approximately 0.16 mm. The laser scan speed ranged from 5 to 100 μm/s. The laser light power ranged from 11 to 19 W.

Photoluminescence (PL) spectra were acquired at room temperature using a micro-PL system. The samples were photoexcited using a 647 nm laser focused on a spot on the sample surface with a diameter of approximately 1 μm. The excitation light power was 2 mW (Laser power 20 mW×1/10 ND filter). Light emission was detected from 1200 to 2200 nm using a cooled, wavelength-extended InGaAs 1024-pixel linear photodiode array (Princeton Instruments: PyLon-IR-2.2) optically coupled to a spectrograph system.

3. Results and discussion

3.1 Effects of scan speed during laser-induced LLPC

Optical images of the GeSn wires fabricated by laser-induced LLPC at different scan speeds are shown in Figure 2. GeSn wires of 5 μm/s have many wire breakings and short Sn precipitates of several micrometers. At this scan speed, the melting time at a certain position of the GeSn wires was approximately 32 s; thus, the Ge atoms aggregated during the long melting time. The interface energy between the liquid Ge and the SiO_2 underlayer was high; Ge atoms easily aggregate during melting on the SiO_2 surface[35]. The wire structure surrounded by the SiO_2 layer effectively suppressed aggregation. However, a long melting time causes the wire to break. Some broken GeSn wires accidentally solidify along the wire, where Sn atoms precipitate at the growth ends.

The GeSn wires at 25 μm/s still have many breaks; however, the number of breaks decreased compared with the wires at 5 μm/s. This was because the melting time decreased. Furthermore, most of the breaks were partially connected because the Sn precipitates lengthened, typically 20 μm. The length of Sn precipitates was proportional to the growth length of the wires[36]. The length of single crystal region in the GeSn wires was estimated to be approximately 300 μm from the length of Sn precipitates. Sn precipitates were distributed from the center to the growth end of the 1 mm-long wires. A low scan speed caused equilibrium growth, indicating a low Sn fraction in the crystalline GeSn wire. The Sn fraction in the melting zone rapidly increased during the scan because it was determined by the difference in the Sn fraction between the amorphous and crystalline GeSn wires, resulting in Sn precipitates during the growth.

In GeSn wires at 50 μm/s, wire breaks were not observed, and most Sn precipitates existed at the growth end of the wires. Thus, the standard crystal growth by zone melting progressed. A fast scan caused non-equilibrium growth, resulting in a high Sn fraction in crystalline GeSn wires. The rapid increase in the Sn fraction in the melting zone and Sn precipitates during the scan were suppressed. Sn precipitates were located at a short distance from the wire end rather than the end. This is because the laser light illuminating the outside of the wire pattern was not absorbed by the samples. The temperature in the melting zone illuminated by the laser light rapidly decreased when the illuminated area reached the pattern

ends.

Similar results were observed for GeSn wires at 100 μm/s, where wire breaks were not observed, and most of the Sn precipitates existed at the growth end of the wires. However, small Sn precipitates were observed in crystalline GeSn wires. This results from the excessive non-equilibrium growth caused by the fast scan speeds. Excess Sn atoms left in the melting zone were segregated on the wires during solidification.

Typical PL spectra of GeSn wires fabricated by laser-induced LLPC with different scan speeds are shown in Figure 3. These spectra were observed at approximately 100 μm upstream (left direction in the figures) from the Sn precipitates because the Sn fraction is high near the upstream side of the Sn precipitates and low near the downstream side of the precipitates. Therefore, these spectra show the feature of the GeSn wire of each scan speed. The GeSn wires at 5 μm/s exhibited many wire breaks, and thus, the whole wires were not single crystals and the variation of PL spectra was large. However, the peak intensity and wavelength was less than 150 and 1800 nm. Thus, certain broken wires were considered as having single crystal structure because the PL intensity was larger than that of bulk Ge.

The peak wavelength increased from 1770 to 2070 nm with an increase in the scan speed. Supposing the tensile strain in the GeSn wires was 0.4%[16),17)], the Sn fractions ranged from 1 to 3.5%. Notably, the Sn fraction of 3.5% for the GeSn wire at 100 μm/s was underestimated because the cutoff wavelength of the detector used in the PL measurements was 2100 nm, and the PL peak wavelength was longer than 2070 nm. The tensile strain originating from the difference in the thermal expansion coefficient between the Ge layers and quartz substrates was expected to be 0.5%. However, suppose the tensile strain was 0.5%, the Sn fraction of the GeSn wire at 5 μm/s was lower than the solid solubility. The increase in the Sn fraction with increasing scan speed reflected the degree of non-equilibrium growth, meaning the Sn fraction can be controlled by changing the scan speed. The PL peak intensity changed depending on the Sn fraction and crystallinity of the GeSn wires. However, the PL peak intensity of the pure Ge crystal obtained using the same setup was much weaker than these peaks. The peak intensity of the GeSn wires at 50 μm/s was approximately 100 times higher than that of the Ge crystal.

Figure 4 shows the PL spectra at the different distances from the Sn precipitates of the GeSn wires at 50 μm/s. The PL peak showed blue shift with the increase in the distance. This

is qualitative agreement with the expectation based on the zone melting kinetics as shown in Fig. 1. In order to achieve uniform Sn fraction in the long range, we need to change the scan speed during LLPC.

3.2 Laser power dependency

Optical images of the GeSn wires fabricated by laser-induced LLPC with a laser power of 19 W are shown in Figure 4. In the image at 25 μm/s, 11 W, shown in Fig. 2, long Sn precipitates were observed from the center to the wire end. However, when the laser power was increased to 19 W, the number of wire breaks increased, and short precipitates were observed at the wire end. High laser power caused the increase in zone temperature and width, resulting in a longer melting time and wire breaks. At 50 μm/s, wire breaks were not observed during the growth at 11 W, and Sn precipitates existed at the wire end. However, long precipitates were observed in the wires fabricated at 19 W, similar to the wires at 25 μm/s, 11 W. Therefore, the Sn fraction in crystalline GeSn wires decreases, causing a rapid increase in the Sn fraction in the melting zone. This might result from the decrease in the degree of non-equilibrium growth owing to the increase in zone temperature.

The differences in the PL spectra caused by the increase in laser power for each scan speed are shown in Figure 5. The PL spectrum of the GeSn wires at 25 μm/s exhibited one of the highest PL peaks, although the variation of the PL spectra increased because of the high laser power. The Sn fractions shown in the figures were estimated from the peak wavelengths. The PL peaks show a blue shift with increasing laser power for both scan speeds. A high laser power increased zone temperature and width; thus, the Sn fraction in the crystalline GeSn wires decreased, resulting in a blue shift in the PL peak. Therefore, the PL peak wavelength can be controlled by varying the laser power.

4. Conclusions

We examined the effects of scan speed and laser power on the crystallinity and optical properties of GeSn wires fabricated by laser-induced LLPC. The PL peak wavelength increased from 1770 to 2070 nm when the scan speed increased from 5 to 100 μm/s, corresponding to an increase in the Sn fraction from 1 to 3.5%, assuming a tensile strain of 0.4%. The increase in laser power caused a blue shift in the PL peaks at scan speeds of 25

and 50 μm/s. We discussed these phenomena based on the growth kinetics of zone melting. Further research is required to precisely and quantitatively control light wavelength, while maintaining high crystal quality.

Acknowledgments

This study was supported by JSPS KAKENHI, Grant Numbers 20H02620, 21K04880, and 22H01528.

References

1) B. Jalali and S. Fathpour, Journal of Lightwave Technology **24**, 4600 (2006).
2) R. A. Soref, Proceedings of the IEEE **81**, 1687 (1993).
3) D. Thomson, A. Zilkie, J. E. Bowers, T. Komljenovic, G. T. Reed, L. Vivien, D. Marris-Morini, E. Cassan, L. Virot, J.-M. Fédéli, J.-M. Hartmann, J. H. Schmid, D.-X. Xu, F. Boeuf, P. O'Brien, G. Z. Mashanovich and M. Nedeljkovic, Journal of Optics **18**, 073003 (2016).
4) R. Soref, IEEE Journal of Selected Topics in Quantum Electronics **12**, 1678 (2006).
5) T. Rudolph, APL Photonics **2**, 030901 (2017).
6) P. Sibson, J. E. Kennard, S. Stanisic, C. Erven, J. L. O'Brien and M. G. Thompson, Optica **4**, 172 (2017).
7) N. C. Harris, R. Braid, D. Bunandar, J. Carr, B. Dobbie, C. Dorta-Quinones, J. Elmhurst, M. Forsythe, M. Gould, S. Gupta, O. Yildirim and K. Zhang, in *2020 Optical Fiber Communications Conference and Exhibition, OFC 2020 - Proceedings* (2020).
8) P. Munoz, P. W. L. van Dijk, D. Geuzebroek, M. Geiselmann, C. Dominguez, A. Stassen, J. D. Domenech, M. Zervas, A. Leinse, C. G. H. Roeloffzen, B. Gargallo, R. Banos, J. Fernandez, G. M. Cabanes, L. A. Bru and D. Pastor, IEEE Journal of Selected Topics in Quantum Electronics **25**, 1 (2019).
9) Y. Zou, S. Chakravarty, C.-J. Chung, X. Xu and R. T. Chen, Photonics Res **6**, 254 (2018).
10) L. Liao, S. Fathololoumi and D. Hui, in *2020 European Conference on Optical Communications (ECOC)* (IEEE, 2020) pp. 1.
11) R. Jones, P. Doussiere, J. B. Driscoll, W. Lin, H. Yu, Y. Akulova, T. Komljenovic and J. E. Bowers, IEEE Nanotechnol Mag **13**, 17 (2019).
12) J. Michel, J. Liu and L. C. Kimerling, Nat Photonics **4**, 527 (2010).
13) S. Wirths, R. Geiger, N. von den Driesch, G. Mussler, T. Stoica, S. Mantl, Z. Ikonic, M. Luysberg, S. Chiussi, J. M. Hartmann, H. Sigg, J. Faist, D. Buca and D. Grützmacher, Nat Photonics **9**, 88 (2015).
14) S. Al-Kabi, S. A. Ghetmiri, J. Margetis, T. Pham, Y. Zhou, W. Dou, B. Collier, R. Quinde, W. Du, A. Mosleh, J. Liu, G. Sun, R. A. Soref, J. Tolle, B. Li, M. Mortazavi, H. A. Naseem and S.-Q. Yu, Appl Phys Lett **109**, 171105 (2016).
15) S. Gupta, B. Magyari-Köpe, Y. Nishi and K. C. Saraswat, J Appl Phys **113**, 073707 (2013).
16) D. Rainko, Z. Ikonic, A. Elbaz, N. von den Driesch, D. Stange, E. Herth, P. Boucaud, M. el Kurdi, D. Grützmacher and D. Buca, Sci Rep **9**, 259 (2019).
17) D. Rainko, Z. Ikonic, N. Vukmirović, D. Stange, N. von den Driesch, D. Grützmacher and D. Buca, Sci Rep **8**, 15557 (2018).
18) J. Liu, X. Sun, R. Camacho-Aguilera, L. C. Kimerling and J. Michel, Opt Lett **35**, 679 (2010).
19) A. Mosleh, S. A. Ghetmiri, B. R. Conley, M. Hawkridge, M. Benamara, A. Nazzal, J. Tolle, S.-Q. Yu and H. A. Naseem, J Electron Mater **43**, 938 (2014).
20) J. Margetis, A. Mosleh, S. Al-Kabi, S. A. Ghetmiri, W. Du, W. Dou, M. Benamara, B. Li, M. Mortazavi, H. A. Naseem, S.-Q. Yu and J. Tolle, J Cryst Growth **463**, 128 (2017).
21) J. M. Hartmann, J.-F. Damlencourt, Y. Bogumilowicz, P. Holliger, G. Rolland and T. Billon, J Cryst Growth **274**, 90 (2005).
22) O. Nakatsuka, N. Tsutsui, Y. Shimura, S. Takeuchi, A. Sakai and S. Zaima, Jpn J Appl Phys **49**, 04DA10 (2010).
23) T. Maeda, W. H. Chang, T. Irisawa, H. Ishii, H. Oka, M. Kurosawa, Y. Imai, O. Nakatsuka and N. Uchida, Semicond Sci Technol **33**, 124002 (2018).

24) H. Oka, T. Amamoto, M. Koyama, Y. Imai, S. Kimura, T. Hosoi, T. Shimura and H. Watanabe, Appl Phys Lett **110**, 032104 (2017).
25) H. Oka, M. Koyama, T. Tomita, T. Amamoto, K. Tominaga, S. Tanaka, T. Hosoi, T. Shimura and H. Watanabe, in *2016 IEEE International Electron Devices Meeting (IEDM)* (IEEE, 2016) pp. 22.1.1.
26) H. Oka, M. Koyama, T. Hosoi, T. Shimura and H. Watanabe, in *2017 Symposium on VLSI Technology* (IEEE, 2017) pp. T58.
27) H. Oka, T. Tomita, T. Hosoi, T. Shimura and H. Watanabe, Applied Physics Express **11**, 011304 (2018).
28) H. Oka, K. Inoue, T. T. Nguyen, S. Kuroki, T. Hosoi, T. Shimura and H. Watanabe, in *2017 IEEE International Electron Devices Meeting (IEDM)* (IEEE, 2017) pp. 16.3.1.
29) Y. Wada, K. Inoue, T. Hosoi, T. Shimura and H. Watanabe, Jpn J Appl Phys **58**, SBBK01 (2019).
30) Z. Liu, J. Wen, X. Zhang, C. Li, C. Xue, Y. Zuo, B. Cheng and Q. Wang, J. Phys. D: Appl. Phys. **48**, 445103 (2015).
31) R. Matsumura, Y. Kai, H. Chikita, T. Sadoh and M. Miyao, AIP Adv. **5**, 067112 (2015).
32) H. Oka, K. Inoue, T. T. T. Nguyen, S. Kuroki, T. Hosoi, T. Shimura and H. Watanabe, in *2017 IEEE International Electron Devices Meeting (IEDM)* (IEEE, 2017) pp. 16.3.1.
33) W. G. Pfann, Metallurgical Reviews **2**, 29 (1957).
34) T. Shimura, R. Yamaguchi, N. Tabuchi, M. Kondo, M. Kuniyoshi, T. Hosoi, T. Kobayashi and H. Watanabe, in *Ext. Abstr. of the 2022 Int. Conf. on Solid State Devices and Materials* (2022) p. 15.
35) T. Hashimoto, C. Yoshimoto, T. Hosoi, T. Shimura and H. Watanabe, Applied Physics Express **2**, 066502 (2009).
36) T. Shimura, M. Matsue, K. Tominaga, K. Kajimura, T. Amamoto, T. Hosoi and H. Watanabe, Appl Phys Lett **107**, 221109 (2015).

Figure Captions

Fig. 1. Schematics of laser zone melting.

Fig. 2. Optical images of GeSn wires fabricated by laser-induced LLPC with different scan speeds. The laser power is 11 W. The arrows indicate wire breaks and Sn precipitates. The scan direction is from left to right.

Fig. 3. PL spectra of GeSn wires fabricated by laser-induced LLPC melting with different scan speeds. Sn fractions are estimated from peak wavelengths assuming a tensile strain of 0.4%. The measurements were performed at room temperature.

Fig. 4. PL spectra at the distances (65, 80, 100, 600 μm) from Sn precipitates of the GeSn wires fabricated by laser-induced LLPC with 50 μm/s scan speed at 11 W laser power. Sn fractions estimated from peak wavelengths assuming 0.4% tensile strain are shown. The measurements were performed at room temperature.

Fig. 5. Optical images of GeSn wires fabricated by laser-induced LLPC with different scan speeds. The laser power is 19 W. The scan direction is from left to right.

Fig. 6. PL spectra of the GeSn wires fabricated by laser-induced LLPC melting with different scan speeds and laser power. Sn fractions were estimated from peak wavelengths assuming a tensile strain of a0.4%. The measurements were performed at room temperature.

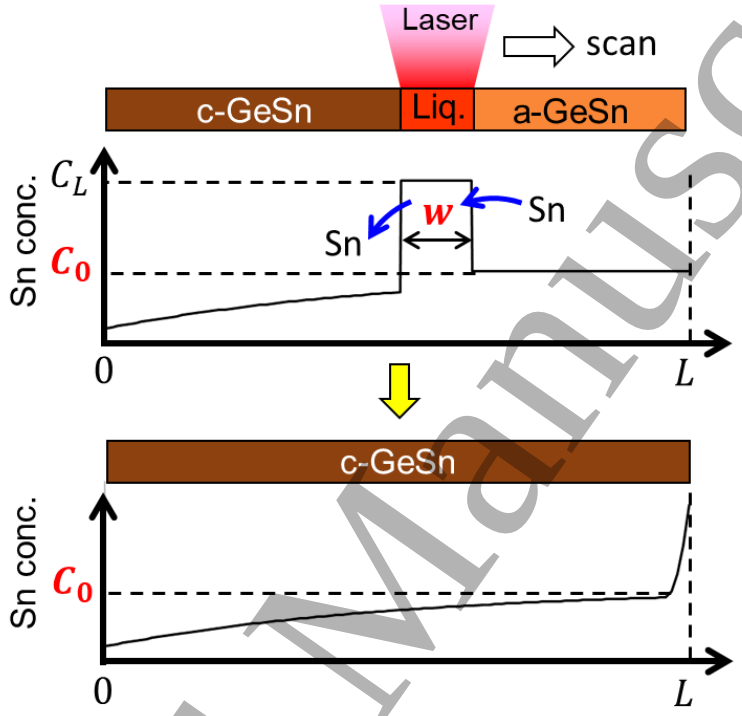

Fig.1.

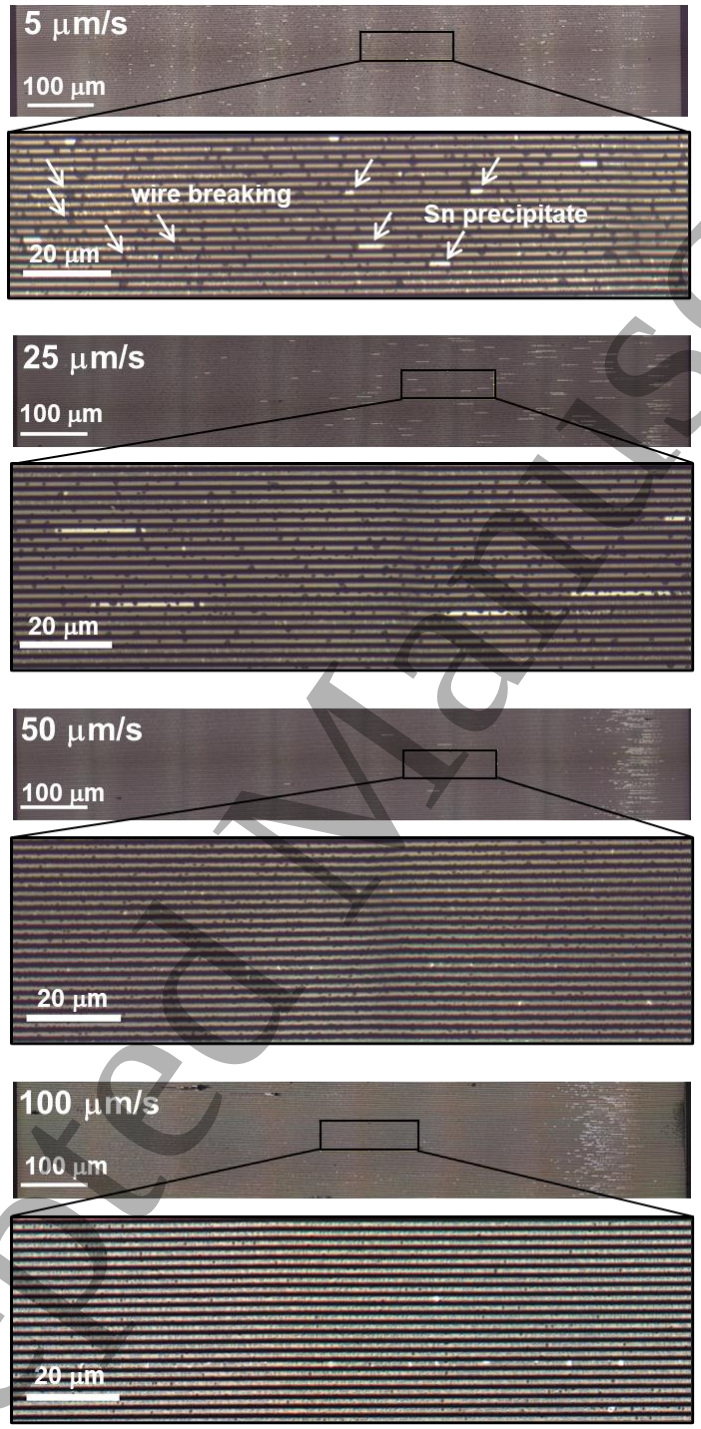

Fig. 2.

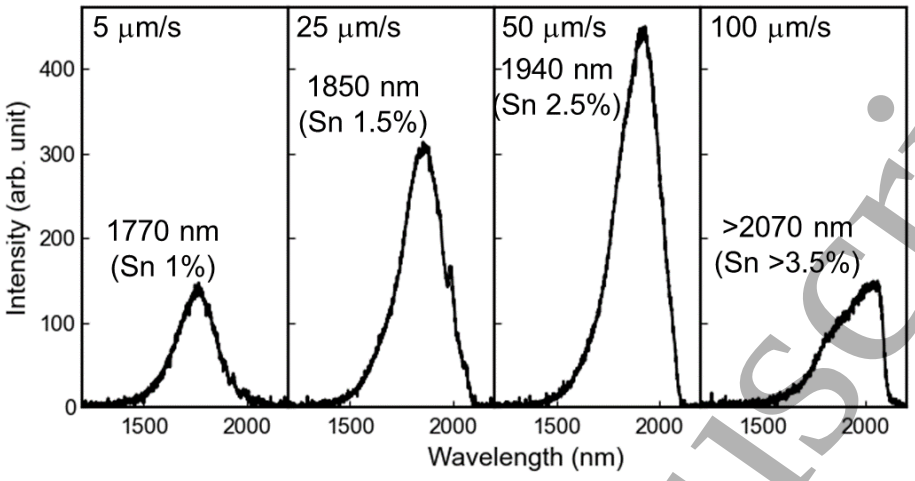

Fig. 3.

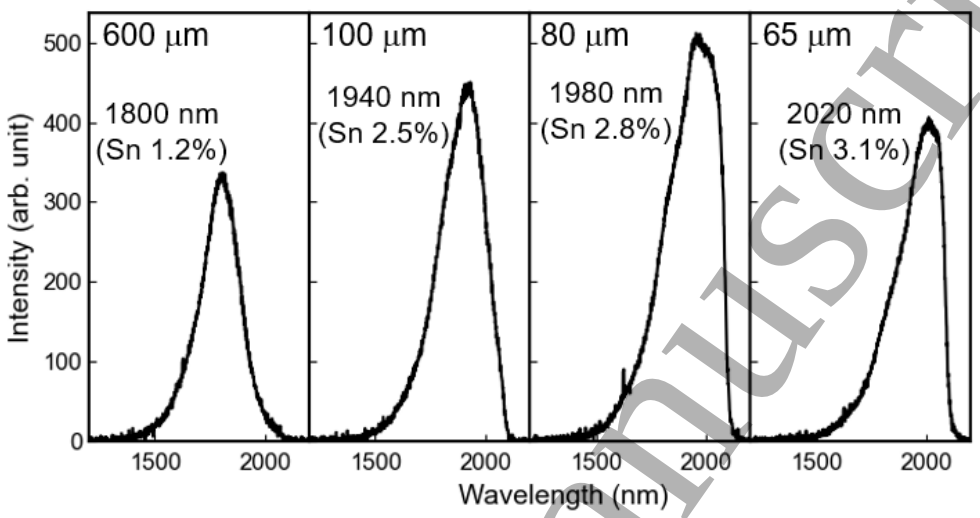

Fig. 4.

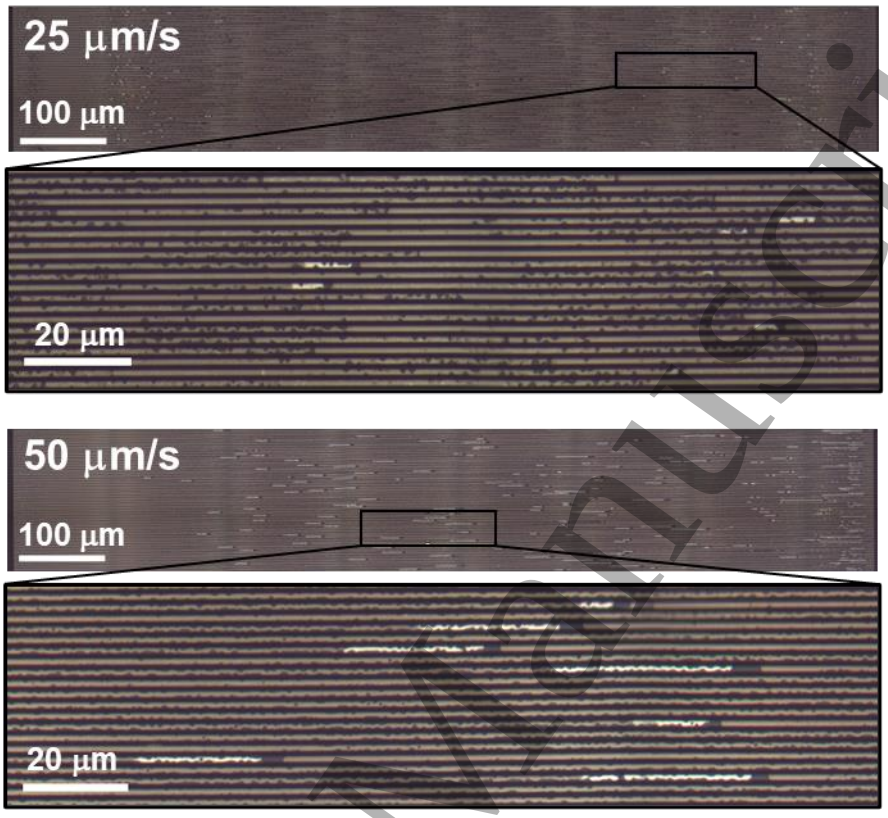

Fig. 5.

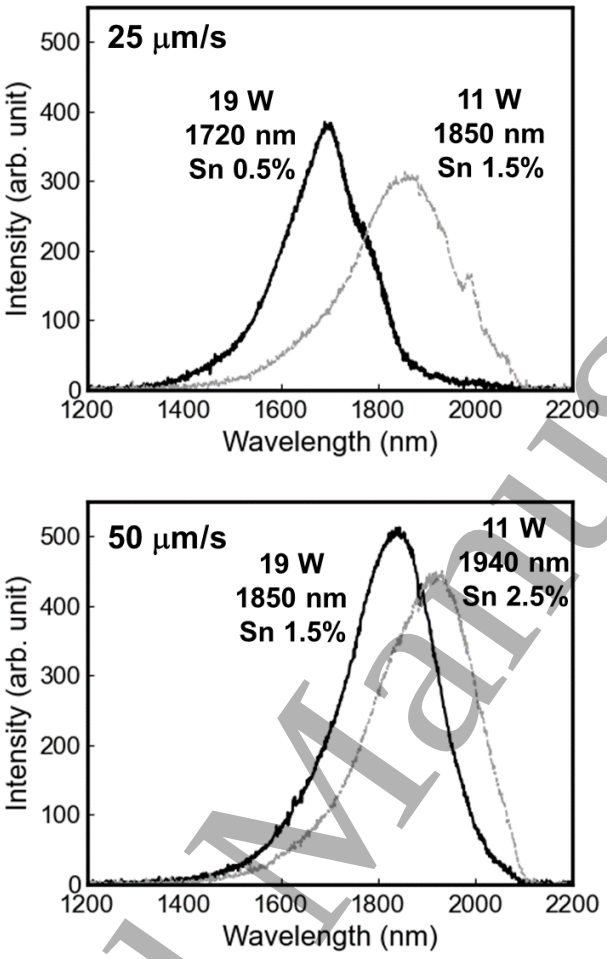

Fig. 6.